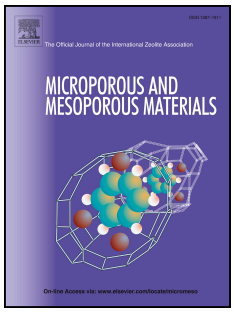

Exploring periodic mesoporous organosilicas for ethane–ethylene adsorption–separation

Marta Bordonhos, Mirtha Lourenço, José R.B. Gomes, Paula Ferreira, Moisés L. Pinto

PII: S1387-1811(21)00101-3

DOI: https://doi.org/10.1016/j.micromeso.2021.110975

Reference: MICMAT 110975

To appear in: *Microporous and Mesoporous Materials*

Received Date: 9 November 2020

Revised Date: 17 January 2021

Accepted Date: 8 February 2021

Please cite this article as: M. Bordonhos, M. Lourenço, José.R.B. Gomes, P. Ferreira, Moisé.L. Pinto, Exploring periodic mesoporous organosilicas for ethane–ethylene adsorption–separation, *Microporous and Mesoporous Materials* (2021), doi: https://doi.org/10.1016/j.micromeso.2021.110975.

M. Bordonhos: Investigation, Visualization. M. Lourenço: Investigation, Visualization. J.R.B. Gomes: Conceptualization, Supervision. P. Ferreira: Conceptualization, Supervision. M. Pinto: Conceptualization, Formal analysis, Validation, Supervision. All authors contributed to writing the original draft and to the review of the manuscript.

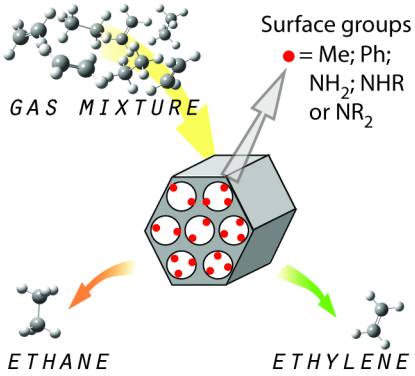

Exploring periodic mesoporous organosilicas for ethane–ethylene adsorption–separation

Marta Bordonhos[a], Mirtha Lourenço[b,c], José R.B. Gomes[d], Paula Ferreira[b], Moisés L. Pinto[a]*

[a] CERENA, Departamento de Engenharia Química, Instituto Superior Técnico, Universidade de Lisboa, 1049-001 Lisboa, Portugal.

[b] CICECO, Departamento de Engenharia de Materiais e Cerâmica, Universidade de Aveiro, Campus Universitário de Santiago, 3810-193 Aveiro, Portugal.

[c] Istituto Italiano di Tecnologia - IIT, Centre for Sustainable Future Technologies (CSFT), Via Livorno, 60, 10144 Torino TO, Italy

[d] CICECO, Departamento de Química, Universidade de Aveiro, Campus Universitário de Santiago, 3810-193 Aveiro, Portugal.

Corresponding Author*

E-mail address: moises.pinto@tecnico.ulisboa.pt

Keywords

Periodic mesoporous organosilicas, silylation, adsorption, ethane–ethylene separation.

Abstract

Ethylene is a core building block in the chemical industry and its separation from ethane is very challenging due to high energy requirements. Adsorption-based processes can be an alternative. In this work, we explore for the first time the application of periodic mesoporous organosilica (PMO) materials, whose surface properties can be tuned with different functional groups. With the aim of correlating the PMO structure with ethane and ethylene adsorption, eight different PMO materials have been prepared, *viz*. the phenylene-bridged PMO, PMO aminated at the organic bridges, and PMO functionalized by silylation of free silanol (inorganic) moieties. High pressure adsorption isotherms were measured, and the separation selectivity and phase diagrams of a binary mixture of ethane and ethylene were estimated. Results have shown that,

overall, the PMO studied tend to be more selective towards ethylene than ethane probably due to the interactions between the quadrupole moment of ethylene and the free silanols in the samples. After silylation, the novel materials presented surfaces with higher affinity towards ethane than those of the pristine material. For the aminated samples, functionalization with primary amines originated materials displaying better selectivity towards ethylene than those functionalized with secondary or tertiary amines.

1. Introduction

Ethylene, the primary building block of several polymers used in the manufacturing of plastics, is one of the most important feedstocks in the petrochemical industry [1–4]. This short-chain olefin is mainly produced via steam cracking of hydrocarbons such as naphtha or ethane. To obtain a high-purity product, ethylene needs to be separated during the final steps of this process from remaining ethane, which can be recycled as feedstock [1–4]. However, ethylene and ethane have similar volatilities and molecular dimensions [4–6] which make their mixtures inherently difficult to separate and a technological challenge for the petrochemical industry [7,8]. Conventionally, this type of separation is done by low-temperature (cryogenic) or high-pressure distillations in large columns (often with more than 100 trays), which significantly increases total costs due to the high energy requirements (*ca*. 85% of the total costs of the steam cracking process are due to ethylene/ethane separation) [2–5]. As such, it is crucial to explore more cost-effective and sustainable alternatives for this energy-intensive separation [4].

Adsorption-based processes, such as pressure or temperature swing adsorptions (PSA or TSA, respectively) or simulated moving bed (SMB), in which an adsorbent material is used to selectively adsorb one of the components in a gaseous mixture, can be regarded as possible alternatives [4,8]. Several classes of porous materials have already been tested for the separation of ethylene from ethane, including zeolitic materials [4,6,9–11], metal-organic frameworks (MOF) [6,12–19], clay-based materials [20–22], silicas [23–25] and carbon-based adsorbents [26–28], with some exhibiting higher selectivity towards ethylene and others towards ethane. Additional examples of porous materials for this separation, particularly of different types of zeolitic materials and MOF, can be found in a comprehensive review by Wang *et al.* [8].

Periodic mesoporous organosilicas (PMO) represent another class of porous materials with interesting properties for this separation. First developed in 1999 by three

independent research groups [29–31], PMO are hybrid porous materials consisting of inorganic silica moieties bridged by organic linkers in layers ordered periodically, typically along the walls of porous channels arranged hexagonally [29–34]. These materials are highly versatile due to their hybrid nature, in which different functional groups can be used during synthesis or post-synthesis modifications, and pore structure, in which different pore sizes and morphologies can be achieved [29–34]. As such, PMO have already been tested in a number of different applications including catalysis, chromatography and adsorption for gas separation [32–34]. However, to the best of our knowledge, PMO have not yet been tested for the adsorptive separation of ethylene from ethane. With this in mind, the aim of this work was to assess the potential of PMO as adsorbents for the separation of ethylene from ethane, as well as to evaluate the effect, on the overall adsorption capabilities of the materials, of different types of modifications in the organic or inorganic moieties in the framework. For this purpose, we tested the performance of a set of PMO adsorbent materials for this separation, using the volumetric method to measure the adsorption equilibrium isotherms of pure ethane and pure ethylene at 25 °C and pressures up to 1000 kPa (10 bar). The experimental adsorption data from the equilibrium isotherms was then implemented in a well-established methodology in order to obtain separation parameters such as selectivity and equilibrium phase diagrams for binary mixtures of these two gases. Eight different types of PMO were tested (*cf.* Scheme 1): a parent phenylene-bridged PMO and three phenylene-bridged PMO functionalized by silylation of free silanol moieties in the framework synthesized for the first time in the present study, and four PMO (three with a phenylene organic bridge and one with a biphenylene organic bridge) functionalized by amination of the organic bridges, with syntheses already described in previous works [35–38].

2. Experimental section

2.1 *Chemicals*

Octadecyltrimethylammonium bromide (ODTMA, 98%, Aldrich), 4,4'-bis(triethoxysilyl)biphenylene (BTEBP, Aldrich, 95%), hydrochloric acid (HCl, 37% v/v, Carlo Erba), nitric acid (HNO_3, 65%, Panreac), sulfuric acid (H_2SO4, 95–97% v/v, Panreac), tin chloride ($SnCl_2$, 98%, Aldrich), isopropylamine ($CH_3CH(NH_2)CH_3$, >99.5%, Aldrich), acetonitrile (99.5%, Sigma), potassium iodide (KI, 99.5%, Riedel-de-

Haën), dichloromethane (CH_2Cl_2, >98%, Sigma-Aldrich), sodium hydrogen carbonate ($NaHCO_3$, 99.55%, Sigma-Aldrich), 2-bromopropane ($CH_3CH(Br)CH_3$, 99%, Aldrich), 3-chloropropionitrile ($ClCH_2CH_2CN$, 98%, Aldrich), chlorotrimethylsilane (Me_3SiCl, 99%, Fluka), chlorotriphenylsilane (Ph_3SiCl, 96%, Aldrich), benzylchlorodimethylsilane ($PhCH_2SiMe_2Cl$, 97%, Aldrich), toluene (98.8%, Aldrich), acetone (PA, Sigma-Aldrich) were purchased from commercial sources. All chemicals were used as received without further purification.

2.2. *PhPMO synthesis and functionalization*

Phenylene PMO (denoted here as PhPMO) was prepared according to the literature procedures [39,40]. The PMO synthesis starts with hydrolysis and condensation of 1,4-bis(triethoxysilyl)benzene (BTEB) precursor [41] in the presence of supramolecular structure directing agent ODTMA. The mixture was stirred at room temperature during 24 h and then subject to 24 h of hydrothermal treatment at 100 °C. Finally, the white solid was filtered and washed. The template was removed using an ethanol/HCl solution under reflux.

The amine-modified phenylene PMO (NH_2PhPMO, Scheme 1) was prepared upon a two-step reaction with very strong acid solutions of i) HNO_3/H_2SO_4 and of ii) $SnCl_2$/HCl under microwave-assisted heating [35].

The *N*-alkylated PhPMO (*i*PrNHPhPMO, Scheme 1), with an isopropyl functionalization inserted in the amino group of NH_2PhPMO sample and *N*,*N*-dialkylated PhPMO (CNPrNPhPMO, Scheme 1), with two propionitrile functional groups inserted in the same amino group of NH_2PhPMO material were prepared using a microwave-assisted procedure [36,37]. The post-synthetic *N*-alkylation and *N*,*N*-dialkylation reactions of 2-bromopropane and 3-chloropropionitrile on NH_2PhPMO, respectively, were made in the presence of KI and acetonitrile at 175 °C.

The amine modified biphenylene PMO (denoted here as NH_2BphPMO, Scheme 1) was prepared using our previous procedure [38], similar to that used for NH_2PhPMO.

The silylation reactions of R–Si–Cl to the free silanols of phenylene-PMO (Scheme 1, denoted here as PhPMO_R), where R can be Me_3, Ph_3 or Me_2Ph, were performed as follows. In a typical synthesis, 300 mg of PhPMO were activated at 110 °C under vacuum. Then, 4.5 mL of dried toluene were added followed by dropwise addition of one of the following R–Si–Cl precursors:

i) 1.5 mL of Me_3SiCl;

ii) 1.5 mg of Ph_3SiCl in 5 mL of toluene;

iii) 1.5 mL of $Me_2Si(CH_2Ph)Cl$.

The mixture was stirred at room temperature during 24 h. After 24 h, the white powder was filtered-off and further washed with acetone, dichloromethane and water. Finally, the resulting PhPMO_R materials were dried at 60 °C.

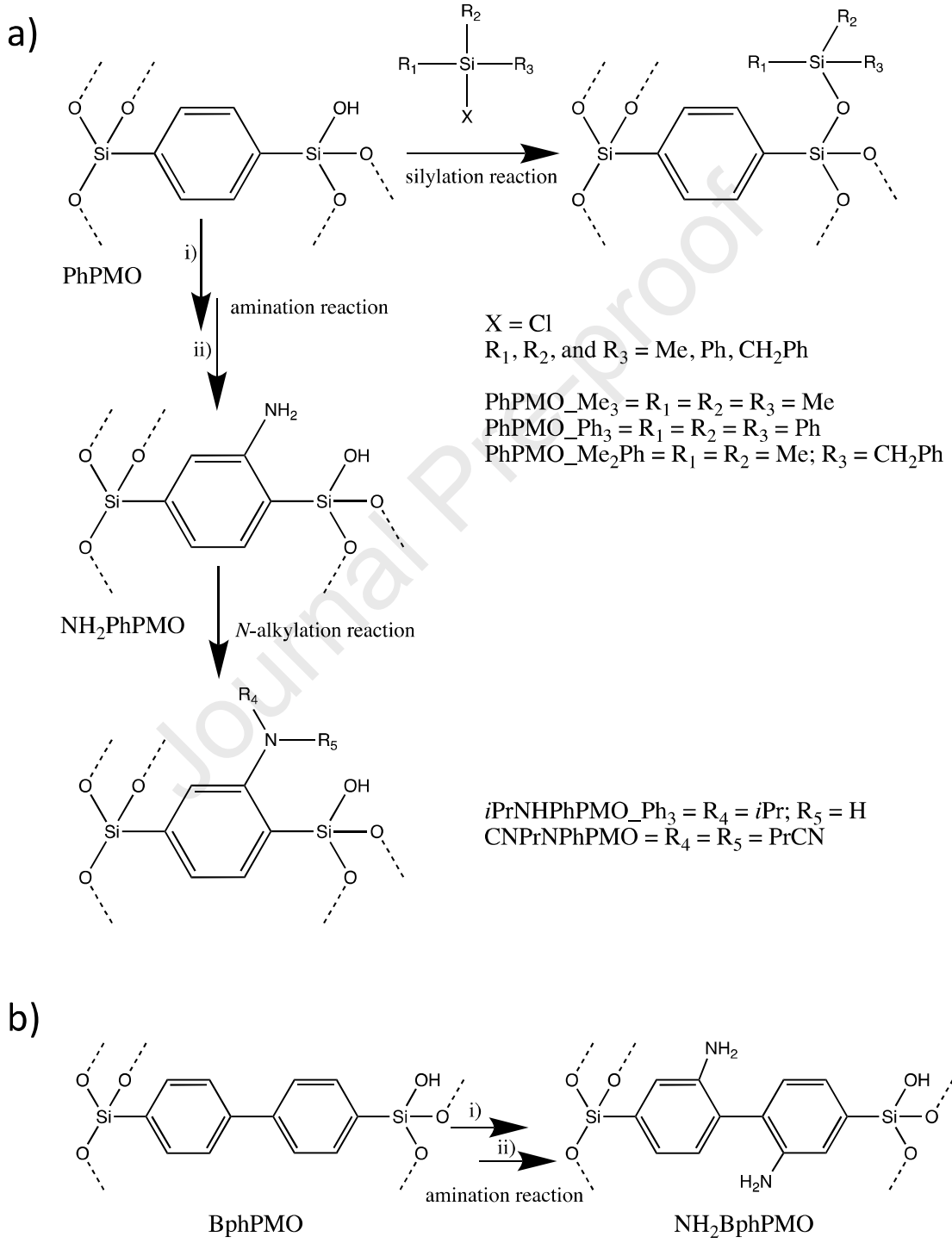

Scheme 1. Schematic representation of the a) silylation reaction of R–Si–Cl to the free silanols of PhPMO; amination reaction and *N*-alkylation reaction of the phenylene-moieties of the PhPMO and b) amination reaction of the biphenylene moieties of the BphPMO materials.

2.3. *Characterization of materials*

The physical and chemical properties of all the synthesized materials were evaluated by powder X-ray diffraction (PXRD), low temperature (-196 °C) nitrogen adsorption-desorption isotherms, ^{29}Si magic angle spinning (MAS) and cross polarized (CP) MAS nuclear magnetic resonance (NMR), ^{13}C CP-MAS NMR and attenuated total reflectance (ATR) Fourier transform infrared (FTIR) spectroscopies, thermogravimetric analysis (TGA) and elemental analysis (EA). Description of the experimental conditions is presented in the Supporting Information (SI) given in Appendix A.

2.4. *Ethane / ethylene adsorption measurements*

Adsorption equilibrium isotherms of ethane (C_2H_6, 99.995%, Air Liquide) and ethylene (C_2H_4, 99.95%, Air Liquide) were measured for the PMO adsorbent samples at 25 °C and in increasing pressures up to *ca*. 1000 kPa (10 bar), using the volumetric method. These experiments were performed in a lab-made stainless-steel volumetric apparatus (Scheme S1, in the SI) with a pressure transducer (MKS, Baratron 627D14TBC1B), and equipped with a vacuum system (Pfeiffer Vacuum, HiCube 80 Eco) that achieves vacuum pressures better than 10^{-2} Pa. Prior to collecting experimental data, all samples were degassed *in situ* at 120 °C for 2 h, under a vacuum pressure of 10^{-4} Pa. This temperature corresponds to a plateau on the TGA curves (Figure S8), and from our previous experience with these materials this procedure is adequate to activate the materials in our vacuum setup. During the experiments, the temperature of the adsorption system and of each sample was controlled via a stirred thermostatic water bath with an accuracy of 0.01 °C (Julabo, MB-5).

Experimental pure-component adsorption equilibrium isotherms for all samples were fitted using the Virial model. The non-ideality of the gas phase was taken into account by using the second and third virial coefficients. Additionally, the experimental excess adsorbed amounts were converted to the absolute adsorbed amounts by taking into account the porous volume of the material and the density of the gas phase using the virial coefficients. Considering the Ideal Adsorbed Solution Theory (IAST) [42], average selectivity values and equilibrium phase diagrams were obtained using a method proposed by Myers [43]. The implementation of this method requires the use of an analytical expression for the experimental adsorption equilibrium isotherms that, in

the scope of this work, is given in the form of a virial equation of state, in which the pressure, *p*, is a function of the adsorbed amount, n^{ads}, as follows:

$$p = \frac{n^{ads}}{K} \exp\left(C_1 n^{ads} + C_2 n^{ads^2} + C_3 n^{ads^3}\right) \quad (1)$$

where *K* is the Henry constant and C_1, C_2, and C_3 are the respective constants of the virial series expansion. A detailed description of the complete implementation of this method can be found in previous works [44,45].

3. Results and discussion

3.1. *Characterization of PMO*

The structural properties of the PMO adsorbents were determined using PXRD and low temperature N_2 adsorption isotherms techniques. Figure 1 displays the PXRD diffraction patterns of PhPMO, PhPMO_Me_3, PhPMO_Ph_3 and PhPMO_Me_2Ph materials. The parent PhPMO has 2*D* hexagonal symmetry (*p6mm*) lattice with a *d* spacing of 4.65 nm for the strong (100) reflection at low-angle (Table 1).

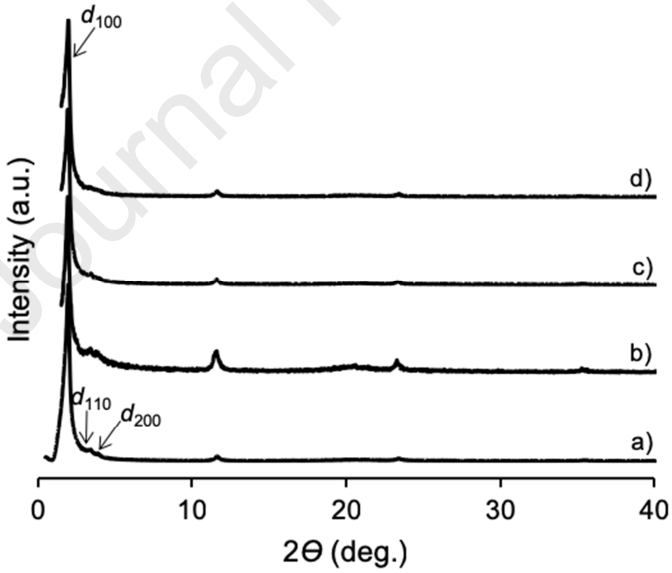

Figure 1. Powder X-ray diffraction patterns of a) PhPMO, b) PhPMO_Me_3, c) PhPMO_Ph_3 and d) PhPMO_Me_2Ph.

In the case of the silylated adsorbents, slight changes are observed in the PXRD (Figure 1) corresponding to the loss of definition of the 2*D* hexagonal arrangement, which is in agreement with the introduction of functional groups into the pores. The d_{100} obtained for the PhPMO_Me_3, PhPMO_Ph_3 and PhPMO_Me_2Ph samples are 4.56, 4.56 and 4.50

nm, respectively (Table 1). A medium-range reflection at d ~ 0.76 nm is observed in all materials which corresponds to the molecular-scale periodicity in the PhPMO pore walls along the channel direction [39]. The parent PMO and all new silylated PMO materials show these peaks at the same d spacing. Thus, the silylation reaction of PMO using different silyl organic reagents is carried out preserving both meso- and molecular- periodicities.

Table 1. Structural and chemical properties of PMO and modified PMO materials.

Samples	d_{100} (nm)	a[a] (nm)	S_{BET}[b] ($m^2 \cdot g^{-1}$)	V_P[c] ($cm^3 \cdot g^{-1}$)	d_P[d] (nm)	C[e] (%)	H[e] (%)	N[e] (%)
PhPMO and silylated PMO								
PhPMO	4.65	5.36	901	0.77	3.6	38.45	2.56	–
PhPMO_Me_3	4.56	5.27	709	0.81	3.2–3.7	38.82	3.00	–
PhPMO_Ph_3	4.56	5.27	709	0.79	3.2–3.7	38.65	2.86	–
PhPMO_Me_2Ph	4.50	5.19	241	0.28	3.2	42.01	3.17	–
Aminated PMO								
NH_2BphPMO	4.67	5.39	588	0.53	3.0	48.52	3.41	4.44
NH_2PhPMO[f]	4.46	5.15	666	0.63	3.4	33.41	3.40	2.30
*i*PrNHPhPMO	4.32	4.99	568	0.74	3.2	38.05	3.44	3.00
CNPrNPhPMO	4.64	5.36	659	0.81	3.3	36.65	2.94	2.94

[a] Unit cell parameter calculated as ($2d_{100}/\sqrt{3}$). [b] The values of the fitted parameters used to calculate the BET surface areas, and the corresponding correlation coefficients, can be found in Table S1, in the SI. [c] BJH Adsorption cumulative volume of pores. [d] Pore diameter obtained from the BJH method with the corrected Kelvin equation, *i.e.*, KJS-BJH method at the maximum of pore size distribution calculated on the basis of adsorption data. [e] Determined by elemental analysis. [f] Values from the sample synthesized in reference [35].

In the case of the aminated materials, the d_{100} of NH_2BphPMO, NH_2PhPMO, *i*PrNHPhPMO and CNPrNPhPMO are 4.67, 4.46, 4.32 and 4.64 nm, respectively (Table 1 and Figure S1, in the SI). The reflection associated to the molecular-scale periodicity is also observed at d ~ 0.76 nm for the aminated PhPMO samples [35–37], while in the case of the NH_2BphPMO material this reflection appears at d ~ 1.9 nm [38] (Figure S1 in the SI). The difference achieved in the molecular-scale periodicity between PhPMO and BphPMO is related with the size of the organic bridges of the PMO, that is bigger in the case of the PMO with biphenylene moieties.

The presence of different organic silyl groups into the pores was confirmed by N_2 adsorption-desorption experiments (Figure S2, in the SI). The pristine PhPMO shows a type IV isotherm [46], characteristic of conventional mesoporous materials such as MCM-41 [47], which corresponds to the presence of a narrow distribution of mesopores with uniform size. The introduction of silylated organic groups into the mesochannels is sustained by a decrease of the specific BET surface area (S_{BET}) and pore volume (V_P)

presented in Table 1 and Figure S2. The PhPMO, PhPMO_Me_3, PhPMO_Ph_3 and PhPMO_Me_2Ph adsorbents have S_{BET} of 901, 709, 709 and 241 $m^2 \cdot g^{-1}$, respectively (Table 1). The decrease in S_{BET} and V_P is much more evident for the PhPMO_Me_2Ph sample, due to the medium bulky nature of this group, which can probably diffuse better into the PMO channels than the Ph_3 silylated functional group (bulkier functional group), during functionalization. A comparison of the pore size distribution (PSD) curves of pristine PhPMO and organic silylated-modified PhPMO adsorbents is revealed in Figure S3, with the values of the pore diameters provided in Table 1, showing maximum shifting from 3.6 to 3.2 nm, respectively. A similar behavior is also observed in the aminated PMO samples as reported in previous works [35–38], where the S_{BET}, V_P and d_P are reduced after amine- and alkylation-functionalization reactions (Figures S4 and S5 in the SI).

Solid-state ^{13}C CP-MAS NMR, ^{29}Si MAS and CP-MAS NMR spectra of PhPMO, PhPMO_Me_3, PhPMO_Ph_3 and PhPMO_Me_2Ph prepared samples are presented in Figures 2 and S6, respectively.

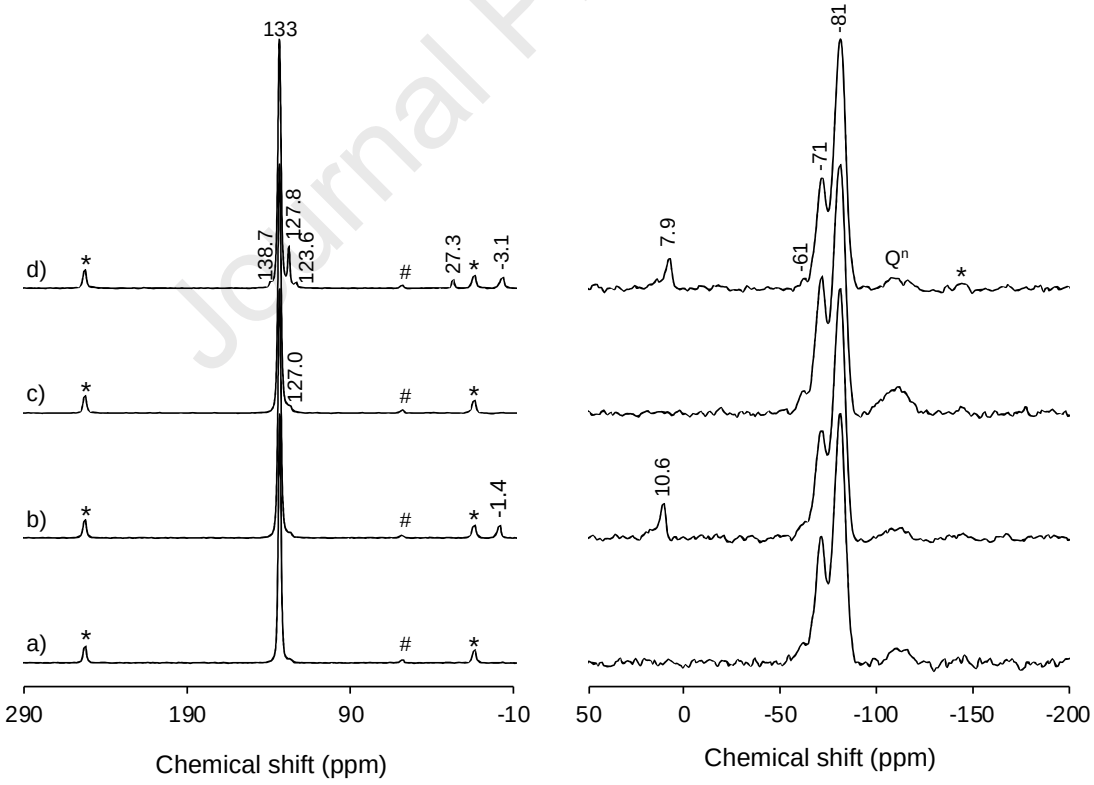

Figure 2. ^{13}C CP-MAS (left) and ^{29}Si MAS (right) NMR spectra of the a) PhPMO, b) PhPMO_Me_3, c) PhPMO_Ph_3 and d) PhPMO_Me_2Ph materials. * denotes the spinning side bands and # denotes the presence of ethanol.

The ^{13}C CP-MAS NMR spectra support the different organic silyl modification of the PhPMO material. The pristine PhPMO (Figure 2a) displays a characteristic resonance at 133 ppm that is related with the aromatic carbon atoms of the phenylene bridge of the PMO material as described in the literature [39]. The incorporation of the $SiMe_3$ groups is detected by the presence of a resonance at *ca*. -1.4 ppm (Figure 2b) corresponding to the methyl groups linked to the silicon atom [48]. The spectrum for PhPMO_Ph_3 (Figure 2c) displays a low intensity peak at 127 ppm that corresponds to inserted phenyl groups. This low intensity indicates a small concentration of $SiPh_3$ groups, which can be explained by a low functionalization due to their bulky nature and concomitant low diffusion along the channels of the PhPMO. The insertion of $SiMe_2Ph$ groups into the PMO was successfully achieved, which is supported by the presence of resonances at 138.7, 127.8 and 123.6 ppm, corresponding to the carbon atoms of the inserted phenylene group, and at -3.1 and 27.3 ppm (Figure 2d), assigned to the carbon atoms of the inserted methyl and Ph–CH_2 moieties, respectively [48].

The grafting of the methyl and phenyl silylated reagents to the free silanols in PhPMO is confirmed by ^{29}Si NMR spectroscopy (Figures 2 and S6). The ^{29}Si MAS and CP-MAS NMR spectra of the parent PhPMO have resonances at *ca.* -81, -71 and -61 ppm corresponding to T^3, T^2 and T^1 (T^m = $SiR(OSi)_m(OH)_{3-m}$) organosiliceous species, respectively. The percentages of the T^m species are presented in Table S2 and were calculated from the deconvolution of the overlapping peaks of ^{29}Si MAS spectra. PhPMO shows 58.7%, 29.1% and 12.2% for T^m species, with m = 3, 2 and 1, respectively. The grafting of the organic silylated functional groups to the T^1 and T^2 silanols of PhPMO is confirmed by the decrease of intensity of the resonances corresponding to these species (Figure S6) when comparing with the T^3 environments (*cf.* Table S2). Nevertheless, in all silylated materials there is still a significant number of remaining T^2 environments. The silylated PMO materials with highest amount of T^3 species and with the lowest quantity of T^1 species is PhPMO_Me_3, followed by PhPMO_Me_2Ph and PhPMO_Ph_3, with 64.6%, 62.1% and 61.1% for T^3 species, and 5.1%, 7.0% and 9.9% for T^1 species, respectively (Table S2). Furthermore, upon silylation it is evident the appearance of an extra peak in the ^{29}Si CP-MAS and MAS NMR spectra of the PhPMO_Me_3 and PhPMO_Me_2Ph materials at high frequency (*ca.* 10.6 and 7.9 ppm, respectively), which may be assigned to M type Me_3***Si***–OSi and Me_2PhCH_2***Si***–OSi silanols, respectively [49]. This resonance is absent in the spectrum of the PhPMO_Ph_3 silylated material. While Q^n species are detected in all materials,

their quantity is clearly more perceptible in the material silylated with the Ph_3SiCl, which is associated to the cleavage of the C–Si bond during the attempt of silylation of the materials surface [50]. The ^{13}C CP MAS and ^{29}Si MAS and CP MAS NMR (not shown) of the aminated PhPMO and BphPMO are in agreement with the ones achieved in our previous works [35–38], showing the successful functionalization of the samples. Table S2 also shows the percentages of the T^m species calculated for these samples. In general, aminated PMO materials present lower amounts of free silanols (both T^1 and T^2 species) than the silylated samples, showing that the amination reaction and posterior amino alkylation seems to promote further hydrolysis and condensation reaction of these species. This behavior is more pronounced in the case of the geminal silanol groups (T^1 species) for the *i*PrNHPhPMO sample (Table S2). As observed for the silylated PMO adsorbents, Q^n species are also more evidenced in the amine-modified PMO samples when compared with the non-modified pristine PMO materials (not shown) [35–38].

The functionalization of the PhPMO with different organic silyl groups was also followed by ATR-FTIR spectroscopy (Figure S7). The C=C stretching modes of the aromatic groups in the framework of the PhPMO are observed in the interval between 1500 and 1680 cm^{-1}. The aromatic C–H stretching bands appear at 3050–3070 cm^{-1} and the methyl C–H stretching bands appear at 2840–3000 cm^{-1}, with the presence of the latter attributed to residual amounts of the surfactant used in the syntheses. The presence of methyl silylated groups upon functionalization is observed on both PhPMO_Me_3 and PhPMO_Me_2Ph materials, by the appearance of a strong, sharp band at 1257 cm^{-1} together with another strong band at 852 cm^{-1}, related to the presence of the C–H bending modes. Additionally, the PhPMO_Me_2Ph material also presents an increase of intensity of the medium-weak bands at 1495 and 1624 cm^{-1} related to the C=C of the phenylene groups. The modification of the PhPMO with the Ph_3SiCl precursor is not convincingly detected by ATR-FTIR spectroscopy, which suggests the slight functionalization of this material with this group. This can be related with the bulky nature of the precursor and its subsequent poor diffusion into the pore channels of the PhPMO.

The TGA of the parent PhPMO and the modified PhPMO materials (Figure S8) shows that all materials display a first weight loss, below 100 °C, which corresponds to desorption of physisorbed water. The grafting of organic silylated groups to the free silanols of the parent PhPMO leads to a reduction of its thermal stability from *ca.* 600

°C to 190 and 200 °C for PhPMO_Me_3 and PhPMO_Ph_3, respectively. The PhPMO material incorporating Ph and Me organic groups (*viz.* PhPMO_Me_2Ph) is thermally stable up to 155 °C.

Table 1 presents the C, H and N percentages in the PMO materials determined by EA. The percentages of C and H in PhPMO are 38.45% and 2.56%, respectively. The grafting of R–Si groups into the PhPMO leads to an increase of both C and H density into the PhPMO, with a carbon content of 38.82%, 38.65%, and 42.01% and a hydrogen content of 3.00%, 2.86% and 3.17% for PhPMO_Me_3, PhPMO_Ph_3 and PhPMO_Me_2Ph materials, respectively. In the case of the aminated PMO materials, the C content increases from NH_2PhPMO < CNPrNPhPMO < *i*PrNHPhPMO < NH_2BphPMO as expected, due to the insertion of the alkyl groups in the case of the modified NH_2PhPMO materials and to the presence of biphenylene groups that replaced the phenylene moieties in the case of the NH_2BphPMO sample. The aminated samples possess between 2.30–4.44% of N, being the lowest N content found for the NH_2PhPMO and the highest one for its homologous NH_2BphPMO material. This difference in N content (almost twice higher in the case of NH_2BphPMO) can be related to the possible bifunctionalization of the benzene groups of the BphPMO (*cf.* Scheme 1) [38].

3.2. *Adsorption of ethane and ethylene*

The pure-component adsorption equilibrium isotherms obtained for ethane and ethylene at 25 °C and up to pressures of 1000 kPa (10 bar) for the eight PMO adsorbent materials can be found in Figure 3 (and individually for each material in Figure S9).

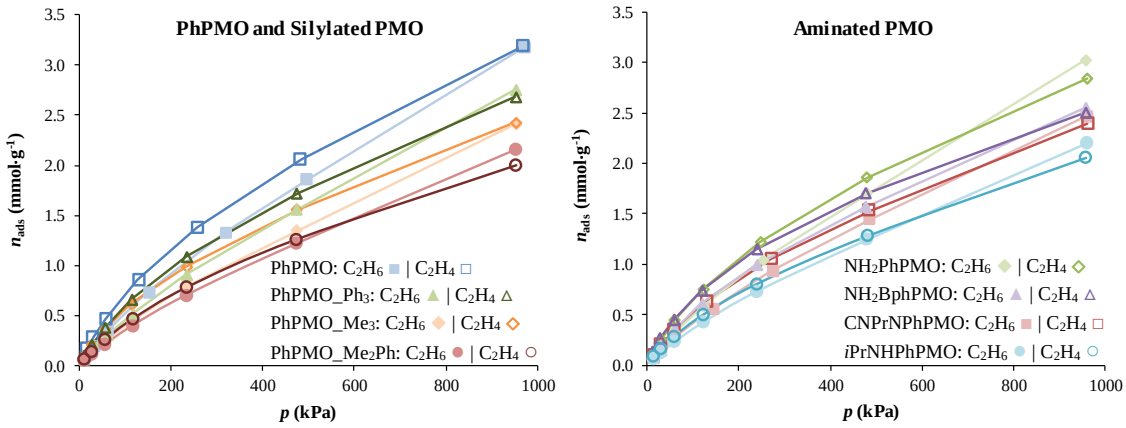

Figure 3. Adsorption equilibrium isotherms of pure ethane (C_2H_6, solid symbols) and pure ethylene (C_2H_4, blank symbols) at 25 °C on PhPMO and silylated PMO (left) and aminated PMO (right). Solid

lines represent the nonlinear least-squares fit of the Virial model to the experimental points. Individual curves for both gases for each material are given in SI (Figure S9).

As can be seen, all eight PMO samples show similar types of adsorption equilibrium isotherms for both gases, and, overall, for pressures below 5 bar ethylene adsorption is higher than ethane in all PMO materials. Regarding the two different sets of functionalizations, silylation of the inorganic free silanol moieties and amination of the organic phenylene bridges of the PMO, for the silylated samples, it can be seen in the isotherms in Figure 3 that PhPMO_Ph_3 is the material adsorbing the highest quantities of ethane and ethylene, followed by PhPMO_Me_3 and lastly PhPMO_Me_2Ph. For the aminated materials it can be seen in the isotherms in Figure 3 that the samples modified with primary amines, NH_2PhPMO and NH_2BphPMO, show higher adsorbed amounts for both gases than CNPrNPhPMO, modified with a tertiary amine, followed by *i*PrNHPhPMO, modified with a secondary amine.

The functionalization of the pores of the PMO decreases the pore volume and surface area (*cf.* Table 1) and this is expected to decrease the adsorption capacity for gases at high pressures, *i.e.,* less adsorption space is available to be filled with the gas molecules. The effect of the functionalization of the samples on surface interaction with ethane and ethylene becomes even more obscured by some differences in functionalization extent and concomitant variation in the surface area decrease. The variation of the surface area on the adsorbed amounts can be compensated by expressing the ethane and ethylene adsorbed amounts per surface area of the material. Thus, to better understand the effect of the functionalization on the adsorption of ethane and ethylene, the adsorption results per mass of material (Figure 3 and Figure S9) and per surface area of material (Figure S10) will be analyzed in more detail to obtain complementary information. Considering first the adsorbed amounts per mass of material, it can be seen in Figure 3 that all functionalized samples, with the exception of NH_2BphPMO which originated from a different parent PMO (*viz.* BphPMO), show an overall decrease in the adsorption of both gases in comparison with the parent PhPMO, which indicates that all the modifications appear to decrease the adsorption capacity of PhPMO for ethane and ethylene. The loss of adsorption potential could, in part, be a consequence of the bulky nature of some functional groups that occupy part of the available pore space (*cf.* Table 1). A good example is PhPMO_Me_2Ph which is, among the samples with the highest degrees of functionalization, the one that has the lowest surface area and pore volume

(*cf*. Table 1) and is the material showing the lowest adsorption of pure ethane and ethylene (*cf*. Figure 3). As a general trend, it can be observed that aminated samples tend to adsorb slightly higher amounts of both gases than silylated samples, despite having lower S_{BET} and V_P values. The silylated samples present higher affinity for ethylene over ethane as a consequence of incomplete functionalization of the parent PMO materials or the occurrence of chemical interactions between the quadrupole moment of ethylene and free silanols in the samples. It can also be observed in Figure 3 that the majority of the PMO materials tend to adsorb higher amounts of ethane than ethylene for pressures in the range of 600–900 kPa and onwards, the exceptions being PhPMO and PhPMO_Me_3, which show higher adsorption of ethylene than ethane until the last data point collected (at *ca.* 1000 kPa). This could be due to the fact that higher pressures will result in higher amounts of gas being adsorbed on the limited pore volume, which may lead to an increase in intermolecular (van der Waals) interactions between gas molecules [7]. The strength of these types of interactions is based on the polarizability of the molecules, and given that the polarizability of ethane (4.47×10^{-24} cm^3) is higher than that of ethylene (4.25×10^{-24} cm^3) [7,51]. This could be the reason why, at higher pressures, there is an overall higher adsorption of ethane over ethylene. Nevertheless, this switch in the adsorption behavior with the increase of the pressure occurs at different pressure values for the different materials, showing that the surface functionalization influences the polarization of the adsorbed ethane molecules [52,53]. For instance, in the case of the silylation modification, the ethane polarization seems to increase in the order PhPMO_Me_3, < PhPMO_Ph_3 < PhPMO_Me_2Ph, with the PhPMO_Me_2Ph starting to adsorb a larger amount of ethane than ethylene at the pressure of approximately 580 kPa. This indicates that the presence of Ph surface groups at the surface of the PMO seems to have a higher impact on polarizing the adsorbed ethane molecules than the Me groups. In this analysis it should be considered that the PMO materials' silanols modification with the Si–Ph_3 groups occurred at lower degree than with Si–Me_2Ph groups, due to the former's bulky nature. On the other hand, in the case of the amino modification of the PMO materials, the secondary amines seem to have a higher influence on the polarization of the ethane molecules than primary or tertiary amines.

To properly reveal the effect of the functionalization on the surface affinity for the gases, the amounts adsorbed per surface area of each material are represented in Figure S10. The silylation on the PhPMO_Me_2Ph resulted in a significant increase of the

amounts adsorbed per surface area (*cf*. it is almost the double at 1000 kPa) comparing to the other materials. Thus, in this case it is clear that, although silylation decreased the amounts adsorbed per mass of material due to the reduction of the pore volume, it increased the surface affinity for the gases. The other silylated samples do not show the same behavior. This difference could be related with the effective introduction of pending Ph on the PhPMO_Me_2Ph sample, that was not achieved in the PhPMO_Ph_3 as discussed in Section 3.1. In the aminated samples, there are not so many marked differences. Nevertheless, a slightly higher interaction of the surface of the samples functionalized with primary amines (NH_2PhPMO and NH_2BphPMO) with the gases is noticed.

To further continue the analysis of the results, the experimental adsorption equilibrium isotherms were fitted with the virial equation of state (1) (solid lines in Figure 3) and the obtained parameters are listed in Table 2.

Table 2. Henry constants (K), virial coefficients (C_1 and C_2) and correlation coefficients (R^2) for the nonlinear least-squares fit of the Virial model to the experimental points for the adsorption of ethane (C_2H_6) and ethylene (C_2H_4) at 25 °C on the studied materials.

Gas	Sample	K (mol·kg^{-1}·kPa^{-1})	C_1 (kg·mol^{-1})	C_2 (kg·mol^{-1})^2	R^2
C_2H_6	PhPMO	6.55×10^{-3}	0.42	- 0.065	0.99958
	PhPMO_Ph_3	5.75×10^{-3}	0.51	- 0.094	0.99965
	PhPMO_Me_3	4.97×10^{-3}	0.59	- 0.128	0.99961
	PhPMO_Me_2Ph	4.18×10^{-3}	0.55	- 0.122	0.99975
	NH_2PhPMO	6.27×10^{-3}	0.48	- 0.084	0.99972
	NH_2BphPMO	7.73×10^{-3}	0.76	- 0.135	0.99949
	CNPrNPhPMO	5.32×10^{-3}	0.56	- 0.108	0.99964
	*i*PrNHPhPMO	4.35×10^{-3}	0.59	- 0.135	0.99984
C_2H_4	PhPMO	1.05×10^{-2}	0.59	- 0.070	0.99974
	PhPMO_Ph_3	8.67×10^{-3}	0.67	- 0.093	0.99974
	PhPMO_Me_3	8.85×10^{-3}	0.88	- 0.150	0.99941
	PhPMO_Me_2Ph	5.50×10^{-3}	0.74	- 0.129	0.99986
	NH_2PhPMO	9.80×10^{-3}	0.66	- 0.083	0.99982
	NH_2BphPMO	1.17×10^{-2}	0.92	- 0.128	0.99967
	CNPrNPhPMO	7.74×10^{-3}	0.79	- 0.132	0.99980
	*i*PrNHPhPMO	5.95×10^{-3}	0.86	- 0.175	0.99980

As can be seen in Table 2, the Henry constants for the adsorption of ethylene are higher than those of ethane for each material tested, which confirms that, especially at lower pressures, the materials tend to adsorb higher amounts of ethylene than ethane. Since in the low-pressure region the adsorption is mainly driven by the interactions with the pore surface, this indicates that in all cases the surfaces interact more strongly with ethylene than with ethane.

In regard to the different materials, NH_2BphPMO has the highest Henry constants for both pure gases, 7.73×10^{-3} mol·kg^{-1}·kPa^{-1} for ethane and 1.17×10^{-2} mol·kg^{-1}·kPa^{-1} for ethylene, which suggests that both gases show the highest affinity for this material, in agreement with the analysis of Figure S10 discussed above. For the other seven samples, the ones showing the highest and lowest Henry constants are the most noteworthy: PhPMO shows the highest Henry constants for both gases, 6.55×10^{-3} mol·kg^{-1}·kPa^{-1} for ethane and 1.05×10^{-2} mol·kg^{-1}·kPa^{-1} for ethylene, as per previous findings that both sets of functionalization (silylation and amination) seem to reduce the adsorption capabilities of PhPMO for ethane and ethylene; PhPMO_Me_2Ph shows the lowest Henry constants for both gases, 4.18×10^{-3} mol·kg^{-1}·kPa^{-1} for ethane and 5.50×10^{-3} mol·kg^{-1}·kPa^{-1} for ethylene, which indicates that both gases show the lowest capacity on this material, despite having a higher degree of functionalization, as already mentioned. However, comparing all the materials, it should be noticed that PhPMO_Me_2Ph has the lowest values for S_{BET}, V_P and d_P (*cf.* Table 1), resulting in the highest adsorbed amounts per surface area (Figure S10).

The evaluation of the separation potential of binary mixtures on the materials was carried out through the implementation of a method proposed by Myers [43], using the virial equation of state (1) fitted to the experimental adsorption data and considering IAST [42]. Using this methodology, it was possible to calculate, for each material, the average selectivity of the separation of ethylene in regard to ethane (C_2H_4/C_2H_6), considering a binary mixture at 25 °C and up to 1000 kPa (Figure 4), and the equilibrium phase diagrams at 25 °C and 500 kPa (Figure S11). In Figure 4, it is possible to see that selectivity for ethylene decreases with increasing pressures for all samples, which indicates that this separation parameter worsens with growing amounts of adsorbed gas and with pressure. Nevertheless, the variation is not significant throughout the pressure range for all materials, the highest variation belonging to PhPMO_Me_3, with values between 1.74 and 1.29.

Regarding the different sets of samples, it is also noticeable that both types of functionalization (silylation and amination) appear to generally reduce the selectivity for ethylene of the parent PhPMO, which goes in accordance with previous adsorption findings, the only exception being PhPMO_Me_3, in which there is an evident increase in the selectivity towards ethylene. For instance, from the silylated PMO materials, PhPMO_Me_3 has the lowest amount of free silanols (*cf.* Table S2) and highest S_{BET} and V_P values (*cf.* Table 1) due to the smaller functional group size (methyl groups). The

combination of these factors seems to influence both adsorption capacity and selectivity of all materials.

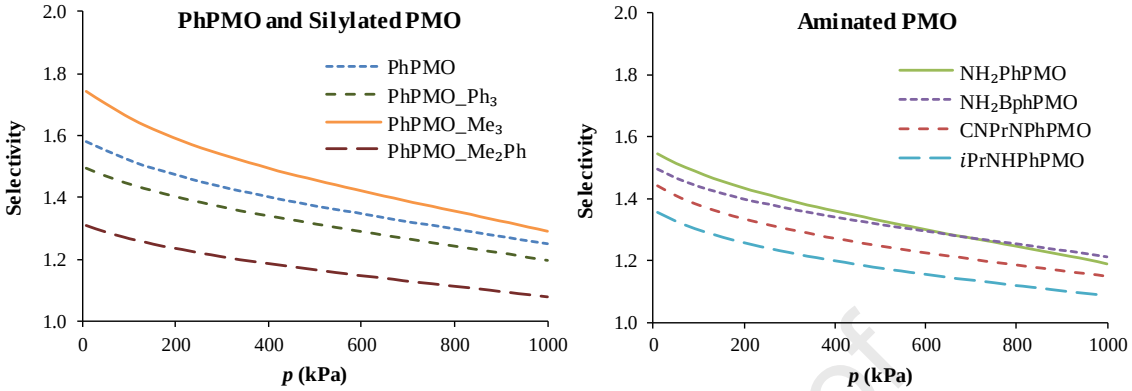

Figure 4. Variation of the average selectivity towards ethylene with pressure at 25 °C on PhPMO and silylated PMO (left), and aminated PMO (right).

Comparing with results reported in the literature for other materials, the PMO materials studied in this work show similar or lower overall selectivities. However, it should be noted that this comparison only gives a general idea of the performance difference between the materials, as selectivity results reported depend on the experimental conditions used (*i.e.*, pressure, temperature, composition and methodology). Several authors reported adsorption experiments up to atmospheric pressure, which may not provide a comprehensive assessment of the materials' performance, particularly for industrial applications. Thus, we opted to compare the selectivity results obtained in this work with reported values close to atmospheric pressure and, when possible, 25 °C. Comparing with zeolitic materials, for NaY a selectivity for ethylene around 3.5 at 100 kPa and 100 °C was reported [4], while for titanium silicates with several different cations, reported selectivities for ethylene for ETS-10 materials varied between *ca.* 1.5 and 13.5 at 100 kPa and 25 °C [10] and for ETS-4 adsorbents between 8 and 67 at 100 kPa and 25 °C [11]. The main challenge in these cases is the very strong binding of ethylene to the materials, which makes it difficult to regenerate the adsorbents and obtain the pure olefin. In the case of MOF adsorbents, reported results vary from ethane- to ethylene-selective materials due to their hybrid chemical nature. For zinc-based MOF materials, selectivities for ethane in the range of 1.4 to 2.7 at 100 kPa and 25 °C [12,17,19] and around 9 at 100 kPa and 43 °C [16] were reported, while for zirconium-based MOF selectivities for ethane between approximately 0.8 and 2.6 at 100

kPa and 25 °C were found [13]. For iron-based MOF materials, selectivities for ethane of 1.9 [15,17] and 4.4 [17] at 100 kPa and 25 °C, and for ethylene of around 13 at 100 kPa and 45 °C [18] were presented. For clay-based adsorbents, selectivities for ethylene between *ca*. 1.8 and 5.3 at 100 kPa and 25 °C [20,21] and 8.6 at 100 kPa and 30 °C [22] were described. For porous silicas, selectivities for ethylene in the range of 1.5 to 4.5 at 100 kPa and 70 °C [23] and 1.6 at 100 kPa and 30 °C [24,25] were observed. Finally, for carbon-based materials, selectivities for ethane reported varied from 1 to *ca*. 2.2 for pressures at or close to 100 kPa and 25 °C [26–28].

Equilibrium phase diagrams were also calculated (Figure S11) and all curves show similar shapes, with no significant differences found between each material's behavior. Considering, as an example, an equimolar gas mixture of ethane/ethylene, all materials show a molar fraction of ethylene in the adsorbed phase between *ca.* 59% and 54%, the former corresponding to the adsorbed molar fraction of ethylene for PhPMO_Me_3 and the latter for PhPMO_Me_2Ph. Considering the silylation effect on the selectivity and separation, it is interesting to note that the introduction of only methyl groups on the surface leads to an increase in affinity for ethylene, comparing with the parent PhPMO, while the introduction of phenyl groups leads to an increase in affinity for ethane. It must be recalled that a complete functionalization is difficult to achieve due to the long channels of the PMO and reagent diffusion constraints. If a higher degree of functionalization could be obtained, the final material would probably have a higher affinity for ethane than for ethylene. For the aminated samples, the functionalization with primary amines seems to give materials (NH_2PhPMO and NH_2BphPMO) with better selectivity (for ethylene) than functionalization with secondary or tertiary amines (*i*PrNHPhPMO and CNPrNPhPMO).

4. Conclusions

Three new silylated PMO were prepared and tested together with five other different PMO materials for the pure-component adsorption of ethane and ethylene, to assess their potential in the separation of a gaseous mixture of these two hydrocarbons. Moreover, it was our intention to correlate their adsorption behavior and distinct chemical environments of the functional groups present at the surface of these materials. Along with the parent PhPMO, two types of functionalization have been tested: silylation of the free silanol moieties and amination of the phenylene bridges of the

PMO.

The results of the pure-component adsorption equilibrium isotherms show that, overall, the adsorption of ethylene is higher than that of ethane for all materials. In the case of the silylated samples, this affinity for ethylene can be attributed to incomplete functionalization of the parent PMO, that leads to the occurrence of chemical interactions between the quadrupole moment of the alkene and remaining free silanols in the samples. Furthermore, it can be seen, in general, that the modifications tend to decrease the adsorption capabilities of the parent PhPMO for both pure gases, which can be related to the structural properties of the functionalized materials, namely the pore volume. The material with the highest Henry constants for pure ethane and ethylene is NH_2BphPMO, indicating that both pure gases show the highest affinity for this material, which is interesting considering it originated from a different type of parent material (BphPMO). Inversely, despite showing a high degree of functionalization, PhPMO_Me_2Ph is the material with the lowest Henry constants for both pure gases, which can be associated to its low values of S_{BET}, V_P and d_P and to the presence of a high amount of free silanol species.

The separation potential of binary mixtures has also been evaluated for each material upon determination of average selectivities and equilibrium phase diagrams. Results show that the average selectivity for ethylene decreases with increasing pressures for all samples, which indicates that the higher the amount of gas mixture fed to the materials, the more difficult it is to selectively adsorb the olefin. Moreover, selectivity results are consistent with the notion that the materials' functionalization appears to reduce the capabilities of PhPMO, with the exception of PhPMO_Me_3, which shows an increase in the selectivity towards ethylene in comparison with the parent PMO. However, at high pressures, the surface functionalization influences the ethane polarization. PMO materials modified by phenylene or secondary amines groups through silylation or organic post-functionalization reactions, respectively, showed to be more selective towards ethane than the other PMO materials, at pressures higher than 600 kPa. This result anticipates a possible application of PhPMO_Me_2Ph and *i*PrNHPhPMO materials on the separation of ethane/ethylene at higher pressures, if the ethane selectivity is desired. In the PhPMO_Me_2Ph case, this may eventually be achieved with a more effective functionalization of the inorganic moiety (*i.e.*, the free silanols).

Declaration of Competing Interest

The authors declare that they have no known competing financial interests or personal relationships that could have appeared to influence the work reported in this paper.

Acknowledgments

This research was financed by Fundação para a Ciência e a Tecnologia (FCT) and developed in the scope of the projects UIDB/04028/2020 & UIDP/04028/2020 (CERENA), and UIDB/50011/2020 & UIDP/50011/2020 (CICECO) financed by Portuguese funds through the FCT/MEC and when applicable co-financed by FEDER under the PT2020 Partnership Agreement. PF, ML and MB acknowledge the grants IF/00300/2015, SFRH/BD/80883/2011 and SFRH/BD/147239/2019, respectively.

Appendix A. Supplementary data

Experimental details of the characterization of the PMOs, namely PXRD, solid state NMR, TGA, ATR-FTIR, elemental analysis. Results of the characterization of the materials. Additional analysis of the adsorption of ethane and ethylene on the PMOs: adsorption isotherms for each individual material, expressed by mass and by surface area of the materials, and isothermal (25 °C)-isobaric (500 kPa) *xy* phase diagrams.

References

[1] S. Matar, L.F. Hatch, Chemistry of Petrochemical Processes, 2nd ed., Gulf Professional Publishing, 2001.

[2] T. Ren, M. Patel, K. Blok, Olefins from conventional and heavy feedstocks: Energy use in steam cracking and alternative processes, Energy. 31 (2006) 425–451. https://doi.org/10.1016/j.energy.2005.04.001.

[3] J.A. Moulijn, M. Makkee, A.E. van Diepen, Chemical Process Technology, 2nd Ed., Wiley, Chichester, United Kingdom, 2013.

[4] A. van Miltenburg, W. Zhu, F. Kapteijn, J.A. Moulijn, Adsorptive Separation of Light Olefin/Paraffin Mixtures, Chem. Eng. Res. Des. 84 (2006) 350–354. https://doi.org/10.1205/cherd05021.

[5] D.M. Ruthven, S.C. Reyes, Adsorptive separation of light olefins from paraffins, Microporous Mesoporous Mater. 104 (2007) 59–66. https://doi.org/10.1016/j.micromeso.2007.01.005.

[6] J. Pires, J. Fernandes, A.C. Fernandes, M. Pinto, Reverse selectivity of zeolites

and metal-organic frameworks in the ethane/ethylene separation by adsorption, Sep. Sci. Technol. 52 (2017) 51–57. https://doi.org/10.1080/01496395.2016.1243130.

[7] R.S. Pillai, M.L. Pinto, J. Pires, M. Jorge, J.R.B. Gomes, Understanding Gas Adsorption Selectivity in IRMOF-8 Using Molecular Simulation, ACS Appl. Mater. Interfaces. 7 (2015) 624–637. https://doi.org/10.1021/am506793b.

[8] Y. Wang, S.B. Peh, D. Zhao, Alternatives to Cryogenic Distillation: Advanced Porous Materials in Adsorptive Light Olefin/Paraffin Separations, Small. 15 (2019) 1–38. https://doi.org/10.1002/smll.201900058.

[9] M. Shi, C.C.H. Lin, T.M. Kuznicki, Z. Hashisho, S.M. Kuznicki, Separation of a binary mixture of ethylene and ethane by adsorption on Na-ETS-10, Chem. Eng. Sci. 65 (2010) 3494–3498. https://doi.org/10.1016/j.ces.2010.02.048.

[10] A. Anson, Y. Wang, C.C.H. Lin, T.M. Kuznicki, S.M. Kuznicki, Adsorption of ethane and ethylene on modified ETS-10, Chem. Eng. Sci. 63 (2008) 4171–4175. https://doi.org/10.1016/j.ces.2008.05.038.

[11] A. Anson, C.C.H. Lin, T.M. Kuznicki, S.M. Kuznicki, Separation of ethylene/ethane mixtures by adsorption on small-pored titanosilicate molecular sieves, Chem. Eng. Sci. 65 (2010) 807–811. https://doi.org/10.1016/j.ces.2009.09.033.

[12] J. Pires, M.L. Pinto, V.K. Saini, Ethane Selective IRMOF-8 and Its Significance in Ethane−Ethylene Separation by Adsorption, ACS Appl. Mater. Interfaces. 6 (2014) 12093–12099. https://doi.org/10.1021/am502686g.

[13] J. Pires, J. Fernandes, K. Dedecker, J.R.B. Gomes, G. Pérez-Sánchez, F. Nouar, C. Serre, M.L. Pinto, Enhancement of Ethane Selectivity in Ethane–Ethylene Mixtures by Perfluoro Groups in Zr-Based Metal-Organic Frameworks, ACS Appl. Mater. Interfaces. 11 (2019) 27410–27421. https://doi.org/10.1021/acsami.9b07115.

[14] C. Gücüyener, J. van den Bergh, J. Gascon, F. Kapteijn, Ethane/Ethene Separation Turned on Its Head: Selective Ethane Adsorption on the Metal-Organic Framework ZIF-7 through a Gate-Opening Mechanism, J. Am. Chem. Soc. 132 (2010) 17704–17706. https://doi.org/10.1021/ja1089765.

[15] Y. Chen, Z. Qiao, H. Wu, D. Lv, R. Shi, Q. Xia, J. Zhou, Z. Li, An ethane-trapping MOF PCN-250 for highly selective adsorption of ethane over ethylene, Chem. Eng. Sci. 175 (2018) 110–117. https://doi.org/10.1016/j.ces.2017.09.032.

[16] P.-Q. Liao, W.-X. Zhang, J.-P. Zhang, X.-M. Chen, Efficient purification of ethene by an ethane-trapping metal-organic framework, Nat. Commun. 6 (2015) 1–9. https://doi.org/10.1038/ncomms9697.

[17] L. Li, R.-B. Lin, R. Krishna, H. Li, S. Xiang, H. Wu, J. Li, W. Zhou, B. Chen, Ethane/ethylene separation in a metal-organic framework with iron-peroxo sites, Science. 362 (2018) 443–446. https://doi.org/10.1126/science.aat0586.

[18] E.D. Bloch, W.L. Queen, R. Krishna, J.M. Zadrozny, C.M. Brown, J.R. Long, Hydrocarbon Separations in a Metal-Organic Framework with Open Iron(II) Coordination Sites, Science. 335 (2012) 1606–1610. https://doi.org/10.1126/science.1217544.

[19] H. Bux, C. Chmelik, R. Krishna, J. Caro, Ethene/ethane separation by the MOF

membrane ZIF-8: Molecular correlation of permeation, adsorption, diffusion, J. Memb. Sci. 369 (2011) 284–289. https://doi.org/10.1016/j.memsci.2010.12.001.

[20] V.K. Saini, M. Pinto, J. Pires, High Pressure Adsorption Studies of Ethane and Ethylene on Clay-Based Adsorbent Materials, Sep. Sci. Technol. 46 (2011) 137–146. https://doi.org/10.1080/01496391003789197.

[21] L.S. Cheng, R.T. Yang, Monolayer Cuprous Chloride Dispersed on Pillared Clays for Olefin-Paraffin Separations by π-Complexation, Adsorption. 1 (1995) 61–75. https://doi.org/10.1007/BF00704146.

[22] N. V. Choudary, P. Kumar, T.S.G. Bhat, S.H. Cho, S.S. Han, J.N. Kim, Adsorption of Light Hydrocarbon Gases on Alkene-Selective Adsorbent, Ind. Eng. Chem. Res. 41 (2002) 2728–2734. https://doi.org/10.1021/ie010546+.

[23] J. Padin, R.T. Yang, New sorbents for olefin/paraffin separations by adsorption via π-complexation: Synthesis and effects of substrates, Chem. Eng. Sci. 55 (2000) 2607–2616. https://doi.org/10.1016/S0009-2509(99)00537-0.

[24] B.L. Newalkar, N. V. Choudary, P. Kumar, S. Komarneni, T.S.G. Bhat, Exploring the Potential of Mesoporous Silica, SBA-15, as an Adsorbent for Light Hydrocarbon Separation, Chem. Mater. 14 (2002) 304–309. https://doi.org/10.1021/cm0106466.

[25] B.L. Newalkar, N. V. Choudary, U.T. Turaga, R.P. Vijayalakshmi, P. Kumar, S. Komarneni, T.S.G. Bhat, Adsorption of light hydrocarbons on HMS type mesoporous silica, Microporous Mesoporous Mater. 65 (2003) 267–276. https://doi.org/10.1016/j.micromeso.2003.08.008.

[26] X. Wang, Y. Wu, X. Zhou, J. Xiao, Q. Xia, H. Wang, Z. Li, Novel C-PDA adsorbents with high uptake and preferential adsorption of ethane over ethylene, Chem. Eng. Sci. 155 (2016) 338–347. https://doi.org/10.1016/j.ces.2016.08.026.

[27] X. Wang, Y. Wu, J. Peng, Y. Wu, J. Xiao, Q. Xia, Z. Li, Novel glucosamine-based carbon adsorbents with high capacity and its enhanced mechanism of preferential adsorption of C2H6 over C2H4, Chem. Eng. J. 358 (2019) 1114–1125. https://doi.org/10.1016/j.cej.2018.10.109.

[28] P. Zhang, X. Wen, L. Wang, Y. Zhong, Y. Su, Y. Zhang, J. Wang, J. Yang, Z. Zeng, S. Deng, Algae-derived N-doped porous carbons with ultrahigh specific surface area for highly selective separation of light hydrocarbons, Chem. Eng. J. 381 (2020) 122731. https://doi.org/10.1016/j.cej.2019.122731.

[29] S. Inagaki, S. Guan, Y. Fukushima, T. Ohsuna, O. Terasaki, Novel Mesoporous Materials with a Uniform Distribution of Organic Groups and Inorganic Oxide in Their Frameworks, J. Am. Chem. Soc. 121 (1999) 9611–9614. https://doi.org/10.1021/ja9916658.

[30] B.J. Melde, B.T. Holland, C.F. Blanford, A. Stein, Mesoporous Sieves with Unified Hybrid Inorganic/Organic Frameworks, Chem. Mater. 11 (1999) 3302–3308. https://doi.org/10.1021/cm9903935.

[31] T. Asefa, M.J. MacLachlan, N.N. Coombs, G.A. Ozin, Periodic mesoporous organosilicas with organic groups inside the channel walls, Nature. 402 (1999) 867–871. https://doi.org/10.1038/47229.

[32] P. Van Der Voort, D. Esquivel, E. De Canck, F. Goethals, I. Van Driessche, F.J. Romero-Salguero, Periodic Mesoporous Organosilicas: from simple to complex

bridges; a comprehensive overview of functions, morphologies and applications, Chem. Soc. Rev. 42 (2013) 3913–3955. https://doi.org/10.1039/c2cs35222b.

[33] S.S. Park, M.S. Moorthy, C.-S. Ha, Periodic mesoporous organosilicas for advanced applications, NPG Asia Mater. 6 (2014) 21. https://doi.org/10.1038/am.2014.13.

[34] J.G. Croissant, X. Cattoën, M. Wong Chi Man, J.O. Durand, N.M. Khashab, Syntheses and applications of periodic mesoporous organosilica nanoparticles, Nanoscale. 7 (2015) 20318–20334. https://doi.org/10.1039/c5nr05649g.

[35] M.A.O. Lourenço, P. Figueira, E. Pereira, J.R.B. Gomes, C.B. Lopes, P. Ferreira, Simple, mono and bifunctional periodic mesoporous organosilicas for removal of priority hazardous substances from water: The case of mercury(II), Chem. Eng. J. 322 (2017) 263–274. https://doi.org/10.1016/j.cej.2017.04.005.

[36] M.A.O. Lourenço, M.J.G. Ferreira, M. Sardo, L. Mafra, J.R.B. Gomes, P. Ferreira, Microwave-assisted N,N-dialkylation of amine-functionalized periodic mesoporous phenylene-silica: An easy and fast way to design materials, Microporous Mesoporous Mater. 249 (2017) 10–15. https://doi.org/10.1016/j.micromeso.2017.04.016.

[37] M.A.O. Lourenço, R. Siegel, L. Mafra, P. Ferreira, Microwave assisted N-alkylation of amine functionalized crystal-like mesoporous phenylene-silica, Dalt. Trans. 42 (2013) 5631–5634. https://doi.org/10.1039/c3dt32011a.

[38] M.A.O. Lourenço, A. Mayoral, I. Díaz, A.R. Silva, P. Ferreira, Amino-modified periodic mesoporous biphenylene-silica, Microporous Mesoporous Mater. 217 (2015) 167–172. https://doi.org/10.1016/j.micromeso.2015.06.026.

[39] S. Inagaki, S. Guan, T. Ohsuna, O. Terasaki, An ordered mesoporous organosilica hybrid material with a crystal-like wall structure, Nature. 416 (2002) 304–307. https://doi.org/10.1038/416304a.

[40] N. Bion, P. Ferreira, A. Valente, I.S. Gonçalves, J. Rocha, Ordered benzene-silica hybrids with molecular-scale periodicity in the walls and different mesopore sizes, J. Mater. Chem. 13 (2003) 1910–1913. https://doi.org/10.1039/b304430k.

[41] R.J.P. Corriu, J.J.E. Moreau, P. Thepot, M.W.C. Man, New Mixed Organic-Inorganic Polymers: Hydrolysis and Polycondensation of Bis(trimethoxysilyl)organometallic Precursors, Chem. Mater. 4 (1992) 1217–1224. https://doi.org/10.1021/cm00024a020.

[42] A.L. Myers, J.M. Prausnitz, Thermodynamics of Mixed-Gas Adsorption, AIChE J. 11 (1965) 121–127. https://doi.org/10.1002/aic.690110125.

[43] A.L. Myers, Equation of State for Adsorption of Gases and Their Mixtures in Porous Materials, Adsorption. 9 (2003) 9–16. https://doi.org/10.1023/A:1023807128914.

[44] M.L. Pinto, J. Pires, J. Rocha, Porous Materials Prepared from Clays for the Upgrade of Landfill Gas, J. Phys. Chem. C. 112 (2008) 14394–14402. https://doi.org/10.1021/jp803015d.

[45] J. Pires, V.K. Saini, M.L. Pinto, Studies on Selective Adsorption of Biogas Components on Pillared Clays: Approach for Biogas Improvement, Environ. Sci. Technol. 42 (2008) 8727–8732. https://doi.org/10.1021/es8014666.

[46] K.S.W. Sing, D.H. Everett, R.A.W. Haul, L. Moscou, R.A. Pierotti, J. Rouquérol, T. Siemieniewaska, Reporting Physisorption Data for Gas/solid Systems with Special Reference to the Determination of Surface Area and Porosity, Pure Appl. Chem. 57 (1985) 603–619. https://doi.org/10.1351/pac198557040603.

[47] J.S. Beck, J.C. Vartuli, W.J. Roth, M.E. Leonowicz, C.T. Kresge, K.D. Schmitt, C.T.W. Chu, D.H. Olson, E.W. Sheppard, S.B. McCullen, J.B. Higgins, J.L. Schlenker, A new family of mesoporous molecular sieves prepared with liquid crystal templates, J. Am. Chem. Soc. 114 (1992) 10834–10843. https://doi.org/10.1021/ja00053a020.

[48] R. Anwander, I. Nagl, M. Widenmeyer, G. Engelhardt, O. Groeger, C. Palm, T. Röser, Surface characterization and functionalization of MCM-41 silicas via silazane silylation, J. Phys. Chem. B. 104 (2000) 3532–3544. https://doi.org/10.1021/jp993108d.

[49] X.S. Zhao, G.Q. Lu, A.K. Whittaker, G.J. Millar, H.Y. Zhu, Comprehensive Study of Surface Chemistry of MCM-41 Using 29Si CP/MAS NMR, FTIR, Pyridine-TPD, and TGA, J. Phys. Chem. B. 101 (1997) 6525–6531. https://doi.org/10.1021/jp971366.

[50] B. Toury, F. Babonneau, Synthesis of periodic mesoporous organosilica from bis(triethoxysilyl)methane and their pyrolytic conversion into porous SiCO glasses, J. Eur. Ceram. Soc. 25 (2005) 265–270. https://doi.org/10.1016/j.jeurceramsoc.2004.08.013.

[51] E. V. Anslyn, D.A. Dougherty, Modern Physical Organic Chemistry, University Science Books, 2006.

[52] C. Schumacher, J. Gonzalez, M. Pérez-Mendoza, P.A. Wright, N.A. Seaton, Design of Hybrid Organic/Inorganic Adsorbents Based on Periodic Mesoporous Silica, Ind. Eng. Chem. Res. 45 (2006) 5586–5597. https://doi.org/10.1021/ie051191n.

[53] V.B. Cashin, D.S. Eldridge, A. Yu, D. Zhao, Surface functionalization and manipulation of mesoporous silica adsorbents for improved removal of pollutants: A Review, Environ. Sci. Water Res. Technol. 4 (2018) 110–128. https://doi.org/10.1039/c7ew00322f.

- Separation of ethane/ethylene on periodic mesoporous organosilicas is studied
- Periodic mesoporous organosilicas tend to be more selective towards ethylene
- Silylation of the materials surface increases the affinity for ethane
- Primary amines functionalization gave better selectivity than secondary or tertiary amines

Declaration of interests

☒ The authors declare that they have no known competing financial interests or personal relationships that could have appeared to influence the work reported in this paper.

☐The authors declare the following financial interests/personal relationships which may be considered as potential competing interests: